CrystEngComm

Accepted Manuscript

This is an *Accepted Manuscript*, which has been through the Royal Society of Chemistry peer review process and has been accepted for publication.

Accepted Manuscripts are published online shortly after acceptance, before technical editing, formatting and proof reading. Using this free service, authors can make their results available to the community, in citable form, before we publish the edited article. We will replace this *Accepted Manuscript* with the edited and formatted *Advance Article* as soon as it is available.

You can find more information about *Accepted Manuscripts* in the Information for Authors.

Please note that technical editing may introduce minor changes to the text and/or graphics, which may alter content. The journal's standard Terms & Conditions and the Ethical guidelines still apply. In no event shall the Royal Society of Chemistry be held responsible for any errors or omissions in this *Accepted Manuscript* or any consequences arising from the use of any information it contains.

ROYAL SOCIETY OF CHEMISTRY

www.rsc.org/crystengcomm

Journal Name

RSCPublishing

ARTICLE

Synthesis, X-ray Characterization and DFT Studies of bis-N-imidazolylpyrimidine salts: the prominent role of hydrogen bonding and anion–π interactions

Cite this: DOI: 10.1039/x0xx00000x

Received 00th January 2012,
Accepted 00th January 2012

DOI: 10.1039/x0xx00000x

www.rsc.org/

Francisca Orvay[a], Antonio Bauzá[a], Miquel Barceló-Oliver[a], Angel García-Raso[a,*], Joan J. Fiol[a], Antoni Costa[a], Elies Molins[b], Ignasi Mata[b] and Antonio Frontera[a,*]

Five new proton transfer compounds, (*bimipyr*H_2)$(Cl)_2$ (**1**), (*bimipyr*H_2)[$(NO_3)(NO_3HNO_3)$] (**2**), (*bimipyr*H_2)$(ZnCl_4)$ (**3**), (*bimipyr*H_2)$(CdCl_4)$ (**4**) and (*bimipyr*H_2)$(HgCl_4)$ (**5**) (*bimipyr* = 4,6-di(1*H*-imidazol-1-yl)pyrimidine) have been synthesized and characterized by elemental analysis, IR and NMR spectroscopy and single crystal X-ray diffraction techniques. The crystallographic analysis revealed that the asymmetric unit of **1** consists of one doubly protonated *bimipyr* molecule, one solvent water molecule and two chloride anions. Conversely, **2** is anhydrous where one counterion is chelated by the $(bimipyrH_2)^{2+}$ molecule and the other anion is solvated by the parent acid forming an independent 'acid salt' counterion $[NO_3HNO_3]^-$. Both compounds exhibit diverse architectures involving hydrogen bonding and anion–π interactions. Compounds **3**, **4** and **5** consist of outer sphere complexes of diprotonated *bimipyr* with $[MCl_4]^{2-}$ as counterion. They have the same molecular composition and compounds **4** and **5** (M = Cd and Hg, respectively) are essentially isomorphous and crystallized in the monoclinic space group P21/n. In the crystal structures of the five salts, N–H···Cl/O and C–H···Cl/O hydrogen bonds as well as anion–π involving aromatic rings and the inorganic anions, and π-stacking interactions are described and analysed by means of density functional theory (DFT) calculations since they play an important role in the construction of three-dimensional supramolecular frameworks. Finally, aggregation studies for compound **1** in solution (DMSO) are also described and discussed.

Introduction

The construction of supramolecular networks with interesting properties and fascinating structures is attracting continuous attention, mainly due to the innovative possibilities how the assemblies are generated through a variety of cooperative noncovalent interactions.[1] The most commonly used strategies in the organization of multi-component supramolecular assemblies are van der Waals, ion pairing, σ-hole[2] and hydrogen bonding interactions[3] and, particularly, those involving aromatic systems like π–π stacking,[4] cation–π,[5] anion–π,[6] etc. Latter interactions[7] have added a new dimension in supramolecular assembly and have emerged as a new concept in anion-transport, anion-sensing and anion-recognition chemistry[8] and transmembrane anion transport.[9] The importance of noncovalent anion–π interaction (i.e the interaction between an electron-deficient aromatic system and a negatively charged species) has been evidenced in gas phase,[10] solid-state,[11] solution[12] and explored in detail by theoretical[13] as well as experimental[14] investigations.

Proton transfer within a hydrogen bond is a fundamental reaction in chemistry, biochemistry and other fields. [15] In particular it plays an important role in enzyme mechanisms, contributing to the catalytic power of enzymes.[16] Polycarboxylic acids and amines are commonly used in crystal engineering since they are excellent building blocks for construction of complex networks by means of proton transfer processes and their coordination to metal ions.[17,18] Moreover, since crystal engineering is a difficult task to conceive due to the delicate nature of the noncovalent forces, the study of the impact of the acidity of reaction media leading to targeted species is still of transcendental importance.

In this study, we report the synthesis, characterization and X-ray crystal structures of several protonated 4,6-di(1*H*-imidazol-1-yl)pyrimidine (*bimipyr*) salts, namely (*bimipyr*H_2)$(Cl)_2$ (**1**), (*bimipyr*H_2)[$(NO_3)(NO_3HNO_3)$] (**2**), (*bimipyr*H_2)$(ZnCl_4)$ (**3**), (*bimipyr*H_2)$(CdCl_4)$ (**4**) and (*bimipyr*H_2)$(HgCl_4)$ (**5**). The theoretical study is devoted to the analysis of the supramolecular assemblies in the solid state. This offers the possibility to elucidate the mechanism of all contributions to

CrystEngComm Accepted Manuscript

molecular recognition and to clarify geometric constraints. It is of particular interest to assign discrete energy values to them since this may help to develop energy scoring functions for crystal design. Taking advantage of DFT calculations and theoretical models we have studied these contributions in several crystal structures (compounds **1**, **2** and **5**) that are useful for the understanding of the noncovalent forces and for rationalizing their influence in the crystal packing.

Experimental

Material and measurements

Chemicals and solvents were purchased from commercial sources (Sigma and Aldrich) and were used as received. Elemental analyses were carried out using Carlo-Erba models 1106 and 1108 and Thermo Finigan Flash 1112 microanalysers. Infrared spectra (KBr pellets) were recorded on a Bruker AMX 300 spectrometer. Proton and carbon chemical shifts in dimethyl sulfoxide solution (DMSO-d_6) were referenced to DMSO-d_6 itself [^{1}H NMR, δ(DMSO) = 2.50; ^{13}C NMR δ(DMSO) = 39.5 ppm]. The ^{13}C NMR spectrum of the diprotonated *bimipyr*H_2 cation is given only for one salt (**1**, *bimipyr*H_2Cl_2) because it does not vary significantly (< 1 ppm) in the other salts **3**-**5**. In addition, the ^{1}H NMR spectrum of the different salts varies depending on the concentration (it has a great tendency to form aggregates, *vide infra*) and, consequently, the concentration used to measure the spectrum is given in the spectroscopic information.

Preparation of the compounds

4,6-di(1*H*-imidazol-1-yl)pyrimidine (*bimipyr*). A solution of 4,6-dichloropyrimidine (1.00 g, 6.71 mmol) and 0.91 g of imidazole (11.36 mmol) in *n*-butanol (20 ml) and triethylamine (2 ml) were refluxed during 24h. After standing and cooling the solution, precipitation of triethylammonium hydrochloride was obtained which was filtered off. The resulting solution was evaporated to dryness and the resulting ocher-colored solid washed with cold water (150 ml) and dried. IR (cm^{-1}): 1661vw, 1592s, 1527vw, 1487s, 1456vw, 1385vw, 1353w, 1328w, 1302m, 1271m, 1255m, 1242m, 1224m, 1124w, 1107m, 1059m, 996m, 973vw, 910w, 882w, 850w, 831w, 782w, 765m, 730w, 652m, 613w, 524w, 462w. ^{1}H-NMR δ(DMSO-d$_6$): 9.01s [1H, C2-H], 8.75s [2H, C2'-H], 8.24s [1H, C5-H], 8.12s [2H, C5'-H], 7.24s [2H, C4'-H]. ^{13}C-NMR δ(DMSO-d$_6$): 159.2 [C2], 156.6 [C4], 135.8 [C2'], 131.1 [C4'], 116.6 [C5'], 96.5 [C5]. ESI-HRMS: [(*bimipyr*)$_2$+Na]$^+$; $C_{20}H_{16}N_{12}Na$: exp: 447.1526; calc: 447.1519.

(*bimipyr*H_2)$(Cl)_2$ (1). (70%) A solution of *bimipyr* 106.0 mg (0.49 mmols) in 15 ml of HCl 0.1 M was refluxed under stirring during 5 hours and then cooled at room temperature. The clear solution yields the corresponding salt as suitable crystals for X-Ray diffraction after three weeks. (C: 39.04; H: 3.86; N: 26.75. Cald for $C_{10}H_{12}Cl_2N_6O$ (%): C: 39.62; H: 3.99; N: 27.72.). IR (cm^{-1}): 481m-2557m (bb), 1664w, 1640w, 1599s, 1573vw, 1540s, 1486w, 1468w, 1430m, 1375w, 1344w, 1310m, 1274m, 1249w, 1212w, 1128w, 1101w, 1086w, 1063w, 995w, 939w, 901w, 852m, 835w, 775w, 765w, 748m, 725w, 626w, 616w, 567w, 496w, 468w, 441w, 405w. *^{1}H-NMR*, δ(300MHz; DMSO-d$_6$; $1\cdot10^{-3}$ M): 9.89s [2H, C2'-H], 9.26s [2H, C2-H], 9.09s [1H, C5-H], 8.62s [2H, C5'-H], 7.77s [2H, C4'-H]. *^{13}C-RMN* δ(300MHz; DMSO-d$_6$): 159.2 [C2], 156.1 [C4], 135.9 [C2'], 124.5 [C4'], 118.4 [C5'], 100.2 [C5].

(*bimipyr*H_2)$[(NO_3)(NO_3HNO_3)]$ (2). Suitable crystals of **2** for X-Ray diffraction were obtained in an unsuccessful attempt to synthesize a coordination complex of *bimipyr* with Co(II) using $Co(NO_3)\cdot6H_2O$ reactant, as follows: a solution of 50 mg *bimipyr* (0.24 mmols) in 12 ml of HNO_3 0.1 M was mixed with a solution of 71 mg of $Co(NO_3)_2\cdot6H_2O$ (0.24 mmols) in 8 ml of HNO_3 0.1 M. The mixture was refluxed at 90ºC during 24 h. After standing and cooling the solution was filtered. The clear solution yields the corresponding salt as suitable crystals for X-Ray diffraction after 24h. IR (cm^{-1}): 3442w, 3102w, 2973w, 1597m, 1572m, 1523m, 1479w, 1425m, 1384s, 1353m, 1313m, 1289m, 1269m, 1186w, 1155w, 1051w, 1029w, 992w, 965w, 890w, 869w, 842w, 823w, 762w, 725w, 626w, 527w, 470w, 439w, 407w. ^{1}H-NMR, δ(300MHz; DMSO-d$_6$; $1\cdot10^{-3}$ M): 9.62s [2H, C2'-H], 9.26s [1H, C2-H], 8.59s [1H, C5-H], 8.40s [2H, C5'-H], 7.76s [2H, C4'-H].

(*bimipyr*H_2)$(ZnCl_4)$ (3). (70%) A solution of *bimipyr* 50.0 mg (0.24 mmols) in 20 ml of EtOH-HCl 1 M was added to a solution of $ZnCl_2$ (32.8 mg) in 2 ml of EtOH. The mixture was refluxed under stirring during 3 days and then cooled at room temperature. The resulting suspension was filtered and the clear solution was allowed to evaporate at room temperature, yielding the salt as suitable crystals for X-Ray diffraction after 45 days. (C: 28.67; H: 2.25; N: 19.97. Cald for $C_{10}H_{10}Cl_4N_6Zn$ (%): C: 28.50; H: 2.39; N: 19.94). IR (cm^{-1}): 3125m, 1596s, 1567w, 1531m, 1478w, 1419m, 1370w, 1360w, 1336m, 1291w, 1270w, 1157w, 1128w, 1096w, 1054w, 989w, 913w, 849w, 769w, 749w, 726w, 626w, 611w, 525w, 466w. ^{1}H-NMR, δ(300MHz; DMSO-d$_6$; $1\cdot10^{-3}$ M): 9.71s [2H, C2'-H], 9.25s [1H, C2-H], 8.84s [1H, C5-H], 8.50s [2H, C5'-H], 7.74s [2H, C4'-H].

CrystEngComm Accepted Manuscript

This journal is © The Royal Society of Chemistry 2012

Table 1. Crystallographic data for complexes **1-5**

	1	**2**	**3**	**4**	**5**
Empirical formula	$C_{10}H_{12}Cl_2N_6O$	$C_{10}H_{11}N_9O_9$	$C_{10}H_{10}Cl_4N_6Zn$	$C_{10}H_{10}Cl_4N_6Cd$	$C_{10}H_{10}Cl_4N_6Hg$
Formula weight	303.16	401.28	421.41	468.44	556.63
Crystal system	Monoclinic	Monoclinic	Orthorhombic	Monoclinic	Monoclinic
Space group	$P2_1/n$	$P2_1/n$	$Ccm2_1$	$P2_1/n$	$P2_1/n$
a (Å)	7.303(2)	9.510(2)	11.395(4)	7.478(2)	7.540(2)
b (Å)	8.599(2)	11.521(3)	14.021(6)	26.697(5)	26.670(5)
c (Å)	21.577(7)	14.622(3)	10.265(4)	8.270(3)	8.200(20)
α (°)					
β (°)	94.32(3)	92.79(2)	90	96.55(2)	97.0(2)
γ (°)					
Z	4	4	4	4	4
V (Å^3)	1351.2(7)	1600.1(6)	1640(1)	1640.2(8)	1636(4)
D_{calc} (Mg m^{-3})	1.490	1.666	1.707	1.897	2.260
μ (mm^{-1})	0.482	0.148	2.149	1.983	10.062
Crystal size	0.36 x 0.27 x 0.15	0.39 x 0.27 x 0.21	0.45 x 0.15 x 0.09	0.36 x 0.21 x 12	0.33 x 0.30 x 0.15
F(000)	624	824	840	912	1040
Total reflections	2445	3261	1800	3167	3903
Unique reflections	2381 (R_{int} = 0.044)	2818 (R_{int} = 0.0496)	1506 (R_{int} = 0.105)	2877 (R_{int} = 0.028)	3565 (R_{int} = 0.0564)
Completeness to θ max (%)	100	99.9	100	100	100
Max. and min. transmission	0.9312 and 0.8456	0.9696 and 0.9447	0.8301 and 0.4447	0.7968 and 0.5355	0.3137 and 0.13560
Data/restraints/parameters	2381 / 3 / 184	2818 / 0 /297	1506 / 1 /103	2877 / 0 / 190	3565 / 0 / 191
θ range (°)	1.89 to 24.97	2.25 to 24.97	2.30 x 24.95	1.53 to 24.97	1.53 to 26.98
Index ranges	$-8 \le h \le 8$	$-11 \le h \le 11$	$0 \le h \le 13$	$-8 \le h \le 8$	$-9 \le h \le 9$
	$0 \le k \le 10$	$0 \le k \le 13$	$0 \le k \le 16$	$0 \le k \le 31$	$0 \le k \le 34$
	$0 \le l \le 25$	$0 \le l \le 17$	$-12 \le l \le 12$	$0 \le l \le 9$	$0 \le l \le 10$
Goodness-of-fit (GOF) on F^2	1.020	1.034	0.996	1.071	1.018
Final R indices	R_1 = 0.048	R_1 = 0.053	R_1 = 0.053	R_1 = 0.042	R_1 = 0.059
[$I \ge 2\sigma(I)$]	wR_2 = 0.103	wR_2 = 0.129	wR_2 = 0.129	wR_2 = 0.095	wR_2 = 0.153
R indices (all data)	R_1 = 0.110	R_1 = 0.103	R_1 = 0.103	R_1 = 0.077	R_1 = 0.101
	wR_2 = 0.123	wR_2 = 0.146	wR_2 = 0.146	wR_2 = 0.107	wR_2 = 0.169
Largest diff. peak and hole (e Å^{-3})	0.287 and -0.364	0.207 and -0.239	0.275 and -0.420	0.599 and -0.692	1.634 and -1.525

(*bimipyr*H_2)($CdCl_4$) (4). (54%) A solution of *bimipyr* 50.0 mg (0.24 mmols) in 20 ml of EtOH-HCl 1 M was added to a solution of $CdCl_2 \cdot H_2O$ (50 mg) in 5 ml of EtOH. The mixture was refluxed under stirring during 2.5 hours and then cooled at room temperature. The resulting suspension was filtered and the clear solution was allowed to evaporate at room temperature, yielding the salt as suitable crystals for X-Ray diffraction after 2 hours. (C: 25.82; H: 2.09; N: 17.83. Cald for $C_{10}H_{10}Cl_4N_6Cd$ (%): C: 25.64; H: 2.15; N: 17.94). IR (cm^{-1}): 3098m, 1644vw, 1594s, 1531m, 1479w, 1422m, 1367w, 1356w, 1336m, 1294w, 1266w, 1154w, 1122w, 1057w, 988w, 870w, 809w, 764w, 753w, 725w, 628m, 615w, 521vw, 471w. ^{1}H-NMR, δ(300MHz; DMSO-d_6; $1 \cdot 10^{-3}$ M): 9.47s [2H, C2'-H], 9.21s [1H, C2-H], 8.58s [1H, C5-H], 8.38s [2H, C5'-H], 7.66s [2H, C4'-H].

(*bimipyr*H_2)($HgCl_4$) (5). (46%) A solution of *bimipyr* 50.0 mg (0.24 mmols) in 20 ml of EtOH-HCl 1 M was added to a solution of $HgCl_2$ (70.5 mg) in 5 ml of EtOH. The mixture was refluxed under stirring during 1 hour and then cooled at room temperature. The resulting suspension was filtered and the clear solution was allowed to evaporate at room temperature, yielding the salt as suitable crystals for X-Ray diffraction after 1 hour. (C: 21.58; H: 1.78; N: 15.12. Cald for $C_{10}H_{10}Cl_4N_6Hg$ (%):C: 21.58; H: 1.81; N: 15.10). IR (cm^{-1}): 3116m, 1606vw, 1593s, 1568m, 1540m, 1524s, 1476m, 1421m, 1370w, 1361w, 1336m, 1290w, 1262w, 1180w, 1154m, 1126m, 1103w, 1051m, 988m, 962vw, 897vw, 840w, 817w, 781vw, 763w, 740w, 726w, 626m, 526vw, 455w, 438vw. ^{1}H-NMR, δ(300MHz; DMSO-d_6; $1 \cdot 10^{-3}$ M): 9.62s [2H, C2'-H], 9.24s [1H, C2-H], 8.69s [1H, C5-H], 8.44s [2H, C5'-H], 7.72s [2H, C4'-H].

X-ray crystallography

X-ray diffraction data of **1**–**5** were collected on an Enraf-Nonius CAD4 diffractometer with graphite monochromated Mo-Kα radiation (λ = 0.71073 A). Data collection was performed at room temperature with ω/2θ scans. Data reduction and Lorentz polarization correction were performed with XCAD4.[19] The empirical absorption correction implemented in DIFABS was applied.[20] All crystal structures were solved by direct methods using SIR2004[21] and refined by full-matrix least squares on F^2 with SHELXL97.[22] Non-hydrogen atoms were refined with anisotropic thermal vibration. In compounds **3**–**5**, a riding model with the anisotropic thermal vibration fixed at 1.2 times U_{iso} of the bonded atom was used for the H-atoms. In **1** the same riding model was applied to H-atoms in the *bimipyr* while those in the water molecule were located in the Fourier differences maps and their coordinates refined. In **2**, all H-atoms were located in the Fourier difference maps and their coordinates and isotropic thermal vibrations were refined. Publication material was generated with WinGX.[23] Crystal data collection and refinement details are given in Table 1.

CrystEngComm Accepted Manuscript

Computational details

All calculations were carried out using the TURBOMOLE version 5.9[24] using the BP86-D3/def2-TZVP level of theory. The molecular electrostatic potential (MEP) surfaces have been computed at the B3LYP/6-31+G* level of theory by means of the Spartan software.[25] The "atoms-in-molecules" (AIM)[26] analysis was performed at the BP86-D3/def2-TZVP level of theory. The calculation of AIM properties was done using the AIMAll program.[27]

Results and Discussion

Synthesis of the compounds

We have synthesized compounds **1-5** by means of the general procedure shown in Scheme 1. The *bimipyr* is easily prepared, in good yield (92 %), from 4,6-dichloropyrimidine and imidazole under refluxing conditions in the presence of a base (Et_3N). Dissolution of *bimipyr* in HCl or HNO_3 (0.1 M) yields the corresponding salts, **1** and **2**, respectively. The (*bimipyr*H_2)(MCl_4) salts **3**-**5** are prepared in moderate yields by refluxing a mixture of *bimipyr* and MCl_2 in EtOH-HCl 1M.

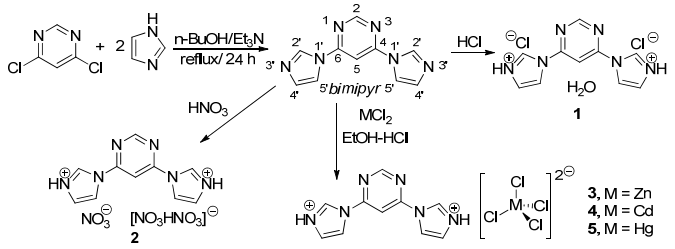

Scheme 1. Synthetic route to compounds **1**-**6**.

We have studied the effect of varying the concentration of the acid (HCl or HNO_3) from 0.1 to 1.0 M on the synthesis of compounds **1** and **2** and the reaction yield is not affected. Therefore for these reactions the impact of the acidity in the 0.1–1.0 M concentration range is negligible.

Aggregation behaviour of (*bimipyr*H_2)$(Cl)_2$ in DMSO

In spite of all salts reported in this study show aggregation properties in DMSO, we have limited the analysis to compound **1** as representative complex. Moreover, compound **1** presents the higher ability to form aggregates. (*bimipyr*H_2)$(Cl)_2$ **1** is only soluble in polar solvents such as DMSO. This solvent give us an indication of the aggregation properties of (*bimipyr*H_2)$(Cl)_2$ in solution. This is supported by the ^{1}H NMR spectrum in *d6*-DMSO, which shows that the chemical shifts of several protons are concentration dependent, thus indicating that some aggregation takes place in this case. Especially relevant is the upfield observed for H2' and H5 hydrogen atoms ($\Delta\delta_{H2'} > 1.0$ ppm) which show large upfield shifts and suggest the direct implication of these hydrogens in the aggregated structure (see Scheme 1 for the numbering). This conclusion is supported by mass spectroscopy (see ESI, Fig. S2). The ESI HRMS spectrum of (*bimipyr*H_2)$(Cl)_2$ show intense peaks at m/z = 461.1839 and 673.2441 amu, assigned to dimer $[(bimipyrH_2)(Cl)]^+$ and trimer $[(bimipyrH_2)(bimipyr)(Cl)]^+$, respectively.

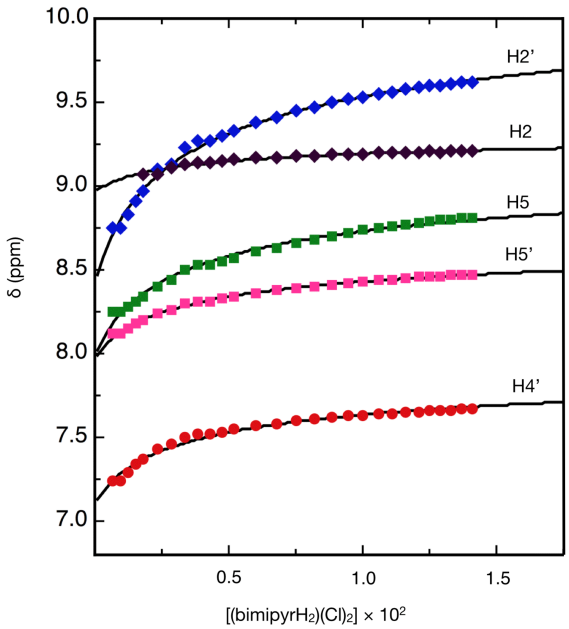

Fig. 1 Concentration dependence of ^{1}H NMR chemical shifts of (*bimipyr*H_2)$(Cl)_2$ in d6-DMSO at ambient temperature (298 *K*) in a range of concentrations from 4.0 × 10^{-4} to 1.4 × 10^{-2} M. Symbols are experimental data points. The curves were calculated by simultaneous nonlinear regression of experimental data by assuming a monomer-dimer model.

To determine the binding constant for the aggregation of the (*bimipyr*H_2)(Cl) salt **1** we studied the concentration dependence of the ^{1}H NMR in a concentration range of 4.0×10^{-4} to 1.4×10^{-2} M. Remarkably, the observed shifts were simultaneously fitted to a monomer-dimer model (2A = A_2) using the program HypNMR[28a] to obtain a dimerization constant K_{dim}= 250 ± 20 M^{-1} (Figure 1). At this point is quite clear from the NMR and mass spectral data that **1** forms dimers even in polar solutions of DMSO. However, the structure of the dimer remains uncertain. In particular, the NMR data agrees well with a dimeric structure composed of two ion-pairs akin to that obtained by X-ray analyses (see, Fig. 3). In the structure of $(\mathbf{1})_2$ two chloride anions are directly hydrogen bonded to C2'-H and C5-H protons, thus accounting for the large upfield field observed for these protons in solution.

Description of the crystal structures

The crystallographic data for compounds **1-5** are shown in Table 1. In addition selected hydrogen bond parameters are given in Tables 2–5.

Crystal structure of (*bimipyr*H_2)$(Cl)_2$ (1). The single crystal X-ray diffraction analysis reveals that (*bimipyr*H_2)$(Cl)_2$ (**1**) crystallizes in the monoclinic system with $P2_1/n$ space group with an asymmetric unit containing two chloride anions one $(\mathbf{bimipyrH_2})^{2+}$ cation and one water molecule that bridges both anions by means of two O1–H···Cl hydrogen bonds (see Fig. 2).

CrystEngComm Accepted Manuscript

This journal is © The Royal Society of Chemistry 2012

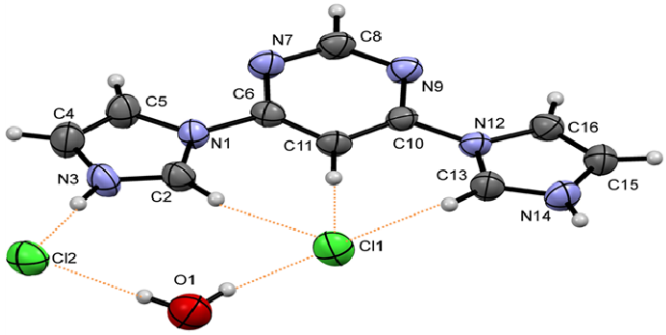

Fig. 2 ORTEP plot of compound **1** and the numbering scheme. The ellipsoids are drawn at the 50% probability level.

In the solid state an interesting self-assembled dimer is formed by means of double N14–H···Cl1 hydrogen bonds (N14-H14···Cl1= 2.19 Å, 176.6º), see blue lines in Fig. 3. In each monomeric unit, the Cl2 anion interacts with the protonated imidazole nitrogen atom N3 and the water molecule, see Table 2. Cl1 is accommodated by the three convergent C–H bonds that are almost equidistant (2.62–2.67 Å) forming three C–H···Cl interactions, as previously observed in related systems.[29] Moreover, it forms a hydrogen bond with the water molecule that bridges it with the other anion (Cl2). The dimers are connected *via* C–H···Cl hydrogen bonds (see red lines in Fig 3, right) resulting in a 1D linear polymeric chain.

Table 2. Hydrogen bonds for **1** [Å and °].

D–H···A	d(D–H)	d(H···A)	d(D···A)	∠(DHA)
N3–H3···Cl2	0.95(4)	2.07(4)	3.025(3)	177(3)
N14-H14···Cl1#1	0.87(4)	2.18(4)	3.054(3)	176(3)
O1-H0···Cl1	0.914(18)	2.339(18)	3.246(3)	171(4)
O1-H1···Cl2	0.902(18)	2.296(18)	3.198(3)	178(3)

#1 -x,-y-1,-z+1

Moreover, the solid-state structure possesses a remarkable supramolecular architecture through two anion–π and one lp–π interactions involving the three rings of *bimipyr* moiety, the chloride and the water molecule (see Fig 3, bottom). The oxygen atom of the water molecule is oriented toward the π-cloud of pyrimidine ring. The separation distance between the ring centroid and the O1 atom is very short 3.14 Å suggesting a significantly strong lp–π interaction. In addition, the halide Cl1 ion interacts with one imidazolium ring with a separation of Cl1···C2 = 3.32 Å, suggesting an anion–π interaction. The other anion Cl2 interacts with π-cloud of the other imidazolium ring. The separation distance between the ring centroid and the Cl2 anion is 3.38 Å. The shortest separation distance reflecting this interaction is Cl2···N12 = 3.447 Å, which is below the sum of the corresponding van der Waals radii. Therefore, the self-assembly involves very unique cooperative anion–π/lp–π/H-bond network in **1** (see Fig 3, bottom). This assembly is further analysed energetically in the theoretical study (*vide infra*) and its importance in the solid state architecture of this compound is illustrated in Fig. 4.

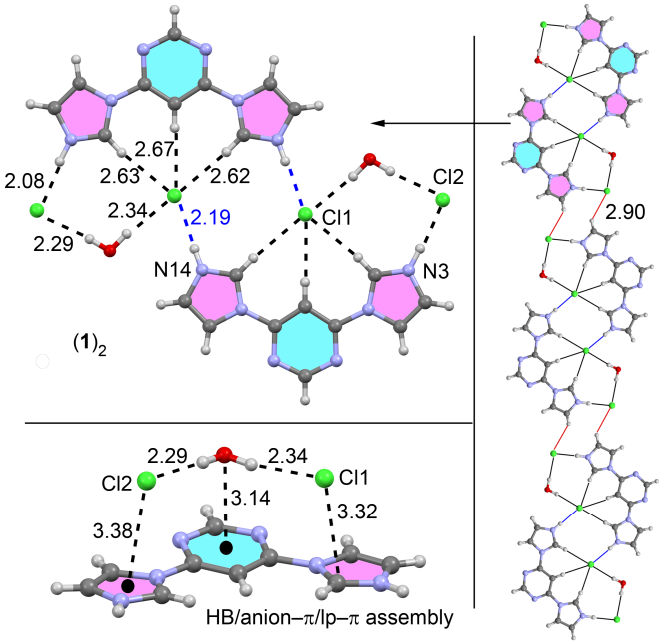

Fig. 3 Several assemblies observed in the X-ray structure of compound **1**. Distances in Å

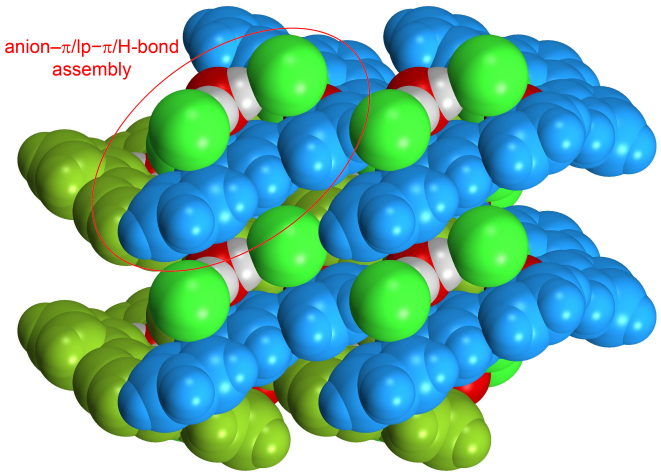

Fig. 4 Space filling representation of the 3D packing of compound 1.

Crystal structure of (*bimipyr*H_2)[(NO_3)(NO_3HNO_3)] (2). The single crystal X-ray diffraction analysis reveals that (*bimipyr*H_2)[(NO_3)(NO_3HNO_3)] (**2**) crystallizes in the monoclinic system with $P2_1/n$ space group with an asymmetric unit containing one nitrate, another nitrate solvated by its parent acid forming an independent 'acid salt' counterion $[NO_3HNO_3]^-$ and the $(bimipyrH_2)^{2+}$ counter-cation (see Fig. 5). The structure of the $[NO_3HNO_3]^-$ array has been previously described in several works, either coplanar as in **2** or nearly orthogonal.[30]

CrystEngComm Accepted Manuscript

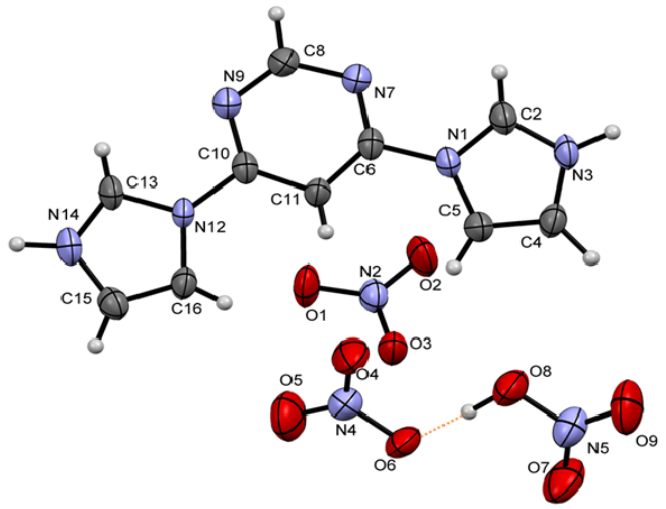

Fig. 5 ORTEP plot of compound **2** and the numbering scheme. The ellipsoids are drawn at the 50% probability level.

The nitrate anion connects two *bimipyr*H_2 cations by means of one oxygen atom (O3) that forms two strong hydrogen bonds with the protonated nitrogen atoms (N3 and N14 of the imidazolium rings (Table 3), generating infinite 1D tapes. These tapes are connected to each other by means of an intricate C–H···O hydrogen bonding network involving the $[NO_3HNO_3]^-$ array (see Fig. 6)

Table 3. Hydrogen bonds for **2** [Å and °].

D–H···A	d(D–H)	d(H···A)	d(D···A)	<(DHA)
N3–H3···O3$^{\#1}$	0.92(3)	1.90(3)	2.815(3)	175(3)
N3–H3···O1$^{\#1}$	0.92(3)	2.44(3)	3.009(4)	120(2)
N3–H3···N2$^{\#1}$	0.92(3)	2.53(3)	3.345(4)	149(2)
N14–H14···O3$^{\#2}$	0.93(4)	1.88(4)	2.811(3)	172(3)
N14–H14···O2$^{\#2}$	0.93(4)	2.32(3)	2.974(3)	127(3)
N14–H14···N2$^{\#2}$	0.93(4)	2.44(4)	3.317(3)	156(3)
O8–H8N···O6	1.03(4)	1.45(5)	2.477(3)	174(4)
O8–H8N···N4	1.03(4)	2.25(4)	3.125(4)	142(3)
O8–H8N···O4	1.03(4)	2.40(4)	2.934(3)	112(3)

#1 x+1/2, -y+1/2, z+1/2; #2 x+1/2, -y+1/2, z-1/2

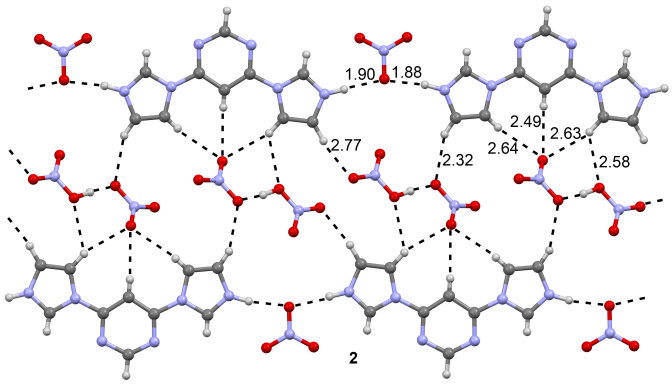

Fig. 6 Infinite 1D tapes connected by the $[NO_3HNO_3]^-$ arrays.

An interesting assembly observed in the solid state structure of 2 is generated by the stacking of the 1D tapes described above. This stacking is crucial for the final 3D structure and it is shown in Fig. 7. It can be described as a combination of anion–π and π–π interactions. The pyrimidine ring of one diprotonated *bimipyr*H_2 cation is involved in parallel-displaced π–π stacking interaction with the protonated imidazole ring of another cation and vice versa with a ring centroid separation of 3.87 Å. These multi π–π stacking interaction are complemented with anion–π interactions involving the other imidazole ring of the *bimipyr*H_2 cation. One oxygen atom (O3) of the anion is oriented toward the π-cloud of the imidazolium ring (Fig. 7). The separation distance between the ring centroid and the O3 is 3.32 Å. This 1D tape described for **2** is also observed in compound **1** (see Fig. 3, left). The main difference is the separation of the monomeric *bimipyr*H_2 units that is higher in **1** due to the presence of a water molecule and the chloride anion connecting the *bimipyr*H_2 units.

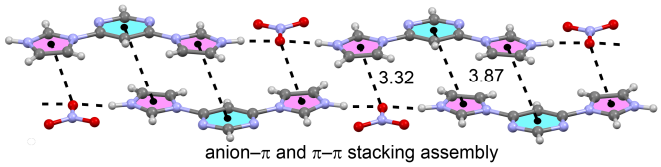

Fig. 7 π-Stacking of the 1D tapes

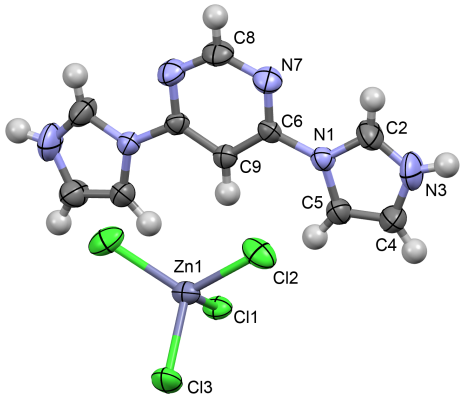

Fig. 8 ORTEP plot of compound **3** and the numbering scheme. The ellipsoids are drawn at the 50% probability level.

Crystal structure of (*bimipyr*H_2)($ZnCl_4$) (3). The ORTEP diagram of compound **3**, which crystallizes in the orthorhombic crystal system, is shown in Fig. 8. The asymmetric unit consists of one half of the $ZnCl_4$ anion and one half of the diprotonated *bimipyr*H_2 cation. The solid-state structure of **3** possesses a remarkable supramolecular architecture through a combination of hydrogen bonding and anion–π interactions (see Fig. 9). The Cl1 atom of the $[ZnCl_4]^{2-}$ anion is accommodated through three convergent C–H···Cl hydrogen bonds similarly to those previously described for **1** (see Fig. 3, top-left). Moreover, this chlorine atom also participates in two additional N3–H···Cl hydrogen bonds with two protonated imidazole rings of two different *bimipyr*H_2 cations (see Fig 9 bottom and Table 4). Finally, the $[ZnCl_4]^{2-}$ anion also establishes a double anion–π interaction where each Cl2 atom interacts basically with the

CrystEngComm Accepted Manuscript

This journal is © The Royal Society of Chemistry 2012

N1–C6 bond (see Fig. 9, top-left). Interestingly, the combination of both H-bonding and anion–π interactions generate infinite zigzag shaped 1D columns in the solid state (see Fig. 9, right)

Table 4. Hydrogen bond for **3** [Å and °].

D–H···A	d(D–H)	d(H···A)	d(D···A)	<(DHA)
N(3)–H(3)···Cl(1)$^{\#1}$	0.86	2.55	3.289(6)	145.1

#1: -1/2+x,1/2+y,z

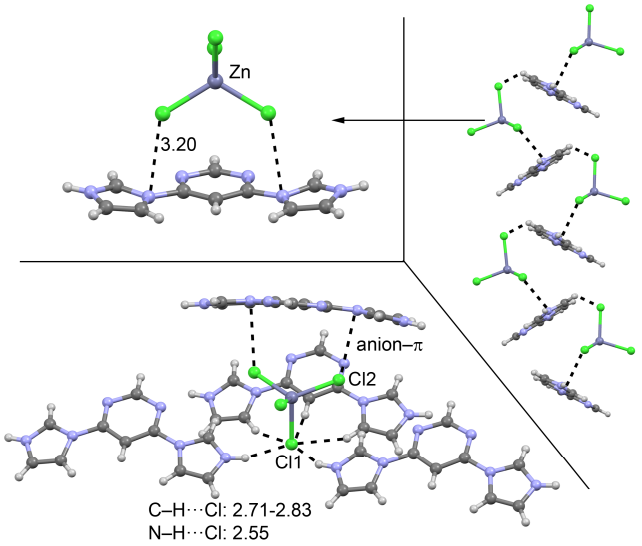

Fig. 9 X-ray fragments of compound **3**. Distances in Å.

Crystal structures of (*bimipyr*H$_2$)(CdCl$_4$) (4) and (*bimipyr*H$_2$)(HgCl$_4$) (5). The compounds **4** and **5** are essentially isomorphous and crystallized in the monoclinic space group P2$_1$/n with the asymmetric unit consisting of the anion $[MCl_4]^{2-}$ and the $(bimipyrH_2)^{2+}$ cation. The ORTEP diagrams of compounds **4** and **5** are shown in Fig. 10.

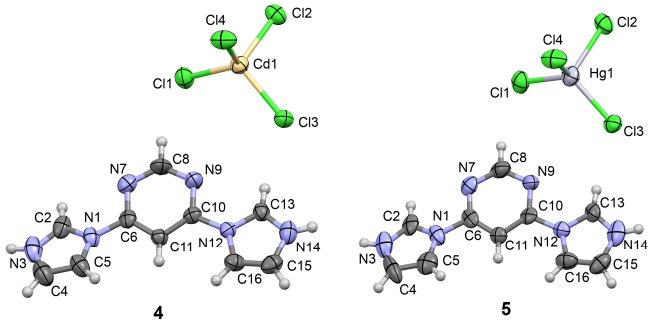

Fig. 10 ORTEP plots of compounds **4** and **5** and the numbering scheme. The ellipsoids are drawn at the 50% probability level.

A significant difference of compounds **4** and **5** with the rest is that the coplanarity of one imidazole ring is lost (aryl-aryl torsion ~20º) in the cation. This is likely due to a combination of two factors, a strong anion–π interaction that involves this imidazole moiety (3.50 Å) and an antiparallel π–π stacking interaction involving the other (almost coplanar) imidazole ring. This combination of interactions generates a self-assembled dimer in the solid state (see Fig. 11) together with an N–H···Cl hydrogen bond (see Table 5). The ability of diazole rings to form antiparallel stacking interactions has been previously reported by us in protonated N-imidazolyl and N-pyrazolyl pyrimidine ligands.[31]

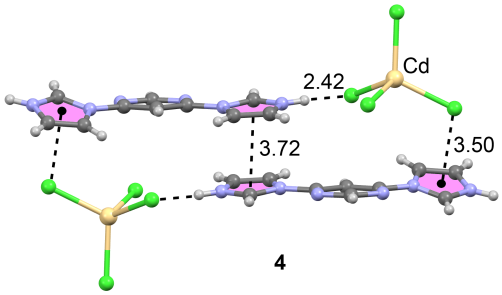

Fig. 11 X-ray structure of the self-assembled dimer observed in compound **4**.

Table 5. Hydrogen bonds for **4** [Å and °].

D–H···A	d(D–H)	d(H···A)	d(D···A)	<(DHA)
N(3)–H(3)···Cl(2)$^{\#1}$	0.86	2.35	3.161(7)	158.3
N(14)–H(14)···Cl(3)$^{\#2}$	0.86	2.42	3.201(6)	151.5

#1: x+3/2,-y+1/2,z+1/2; #2: -x+1,-y,-z+1

These self-assembled dimers propagate in the solid state forming infinite ladders by means of the formation of anion–π/π–π/π–anion assemblies (see Fig. 12), producing the occurrence of an interesting blend of weak forces in the solid-state that act simultaneously. This combination of anion–π/π–π/π–anion interactions has been recently described in bromide salts of terpyridine derivatives.[31,32] In addition, similar assemblies involving two different anions and protonated aminopyridine have been also described. In particular the ability of different anions (nitrate, perchlorate and hexafluorophosphate) to generate this type of supramolecular associations has been recently studied both theoretically and experimentally.[33]

CrystEngComm Accepted Manuscript

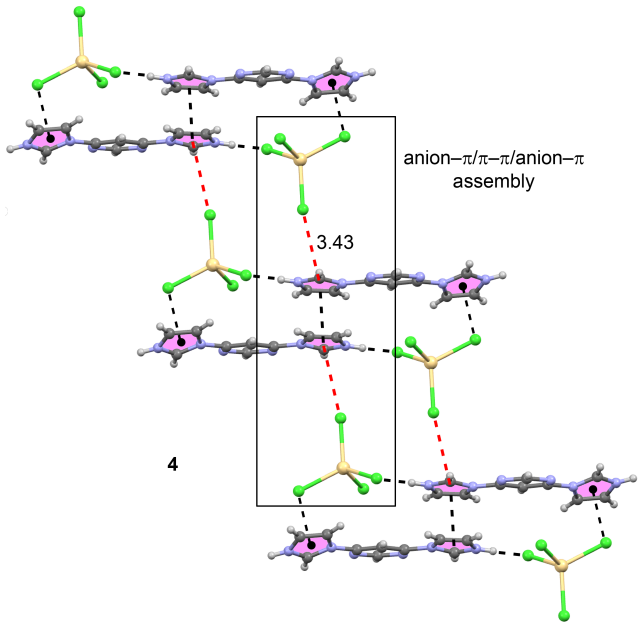

Fig. 12 Partial view of the X-ray structure of compound **4**. Distance in Å.

Theoretical Study

In this part of the manuscript we analyse the interesting and uncommon noncovalent interactions and assemblies observed in the solid state architectures of compounds **1**–**4** described above. In particular we have mainly focused our attention to the anion–π interactions that have been observed in the crystal structures and have a strong influence on the crystal packing. Clearly, the hydrogen bonding interactions (N^+–H···Cl/O) play an important role in the final architecture of the X-ray structures of **1**–**5** (*vide supra*). However, we have mainly concentrated the theoretical analysis in the interactions that are less studied in the literature.

In an effort to rationalize the anion–π and H-bonding interactions concerning the three convergent C–H bonds, we have computed the molecular electrostatic potential surface (MEPS) of the (*bimipyr*H_2)$(Cl)_2$ since it is a neutral system and allows to evaluate other interactions apart from the strong electrostatic interactions between the counter-ions (protonated nitrogen atom of imidazol and chloride). We have used two different conformations (see Fig. 13) because both are observed in the solid state of compounds **1**–**5**. From the MEP surfaces some interesting issues arise. First, the most electrostatically positive region (blue color) is located in the molecular plane where the three C–H bonds converge. This result is in sharp agreement with the solid state structure of all compounds that present either the anion (Cl) or an atom of the polyatomic anion (NO_3^-, MCl_4^{2-}) Second, there is also a positive potential isocontour (+70 kcal/mol) over the six membered pyrimidinic ring, which is more extended in the "*syn*" conformer. Third, there are also positive potential isocontours over the five-membered imidazole rings. Interestingly, the isocountour in the "*syn*" conformer is approximately located over the C2/C13 (see Fig. 2 for the numbering scheme) carbon atoms, which is approximately the position of the anion (Cl1) in the solid state (see Fig. 2, bottom).

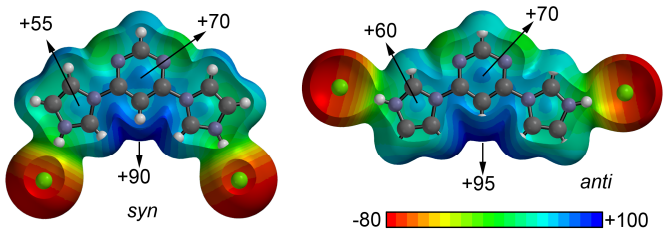

Fig. 13 MEPS surfaces of compound **1**. Energies in kcal/mol.

In compound **1**, using the crystallographic coordinates we have evaluated the contribution of the different interactions observed in the solid state, using the neutral (*bimipyr*H_2)$(Cl)_2$ unit for the calculations. In Fig 14 we show the fragment used for the calculations. The interactions are large and favorable due to the dicationic nature *bimipyr*H_2 moiety in spite of including the counter-ions in the models. The trifurcated H-bonding is more favorable (ΔE_1 = –42.2 kcal/mol) than the anion–π interaction (ΔE_2 = –37.4 kcal/mol), in agreement with the MEPS analysis. The interaction energy computed for the assembly is also large and negative (ΔE_3 = –74.7 kcal/mol) confirming the importance of this assembly in the solid state architecture of compound **1** (see Fig. 4).

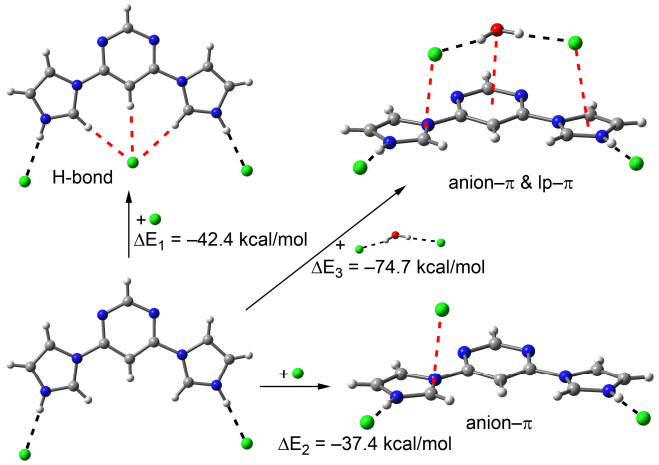

Fig. 14 Theoretical models and binding energies computed to evaluate the noncovalent interactions in compound **1**

Similarly to compound **1**, in **2** we have also analyzed the energetic features of the H-bonding and anion/lp–π interactions (see Fig 15) The trifurcated H-bonding is also more favorable (ΔE_4 = –50.3 kcal/mol) than the anion/lp–π interaction (ΔE_5 = –37.9 kcal/mol) and even more favorable than the trifurcated H-bond in compound **1** (ΔE_1 = –42.2 kcal/mol) likely due to the shorter pyrimidinic C–H···anion distance in **2** (see Figs. 3 and 6).

CrystEngComm Accepted Manuscript

This journal is © The Royal Society of Chemistry 2012

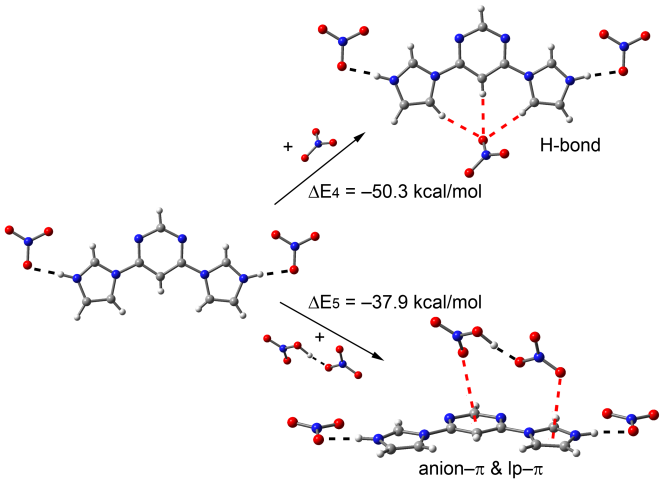

Fig. 15 Theoretical models and binding energies computed to evaluate the noncovalent interactions in compound **2**.

In compound **3**, we have also evaluated the trifurcated hydrogen bonding and the anion–π interactions by computing the formation energy of the trimer represented in Fig. 16 considering either that the anion–π complex has been previously formed (ΔE_6) or that the trifurcated H-bonding complex has been previously formed (ΔE_7). Using this method, we evaluate the individual interactions using the neutral salt (*bimipyr*H_2)($ZnCl_4$). The result is consistent with the previously observed for compounds **1** and **2** and the MEPS analysis. That is the H–bonding complex formation is more favored (ΔE_7 = –85.4 kcal/mol) than the anion–π interaction (ΔE_5 = –66.4 kcal/mol). In absolute value, both interactions are greater than those computed for **1** and **2** due to the doubly charged interacting anion.

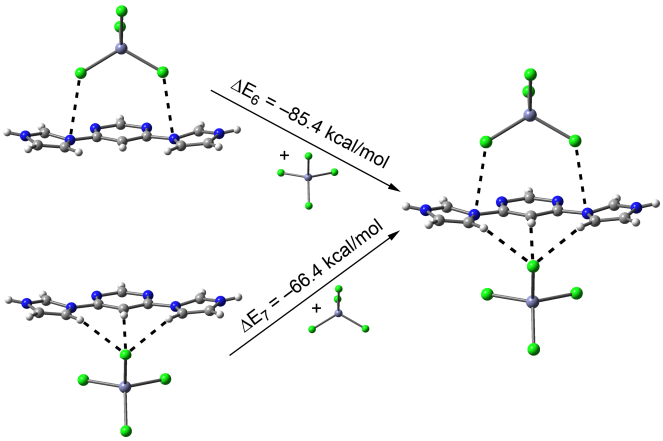

Fig. 16 Theoretical models and binding energies computed to evaluate the noncovalent interactions in compound **3**.

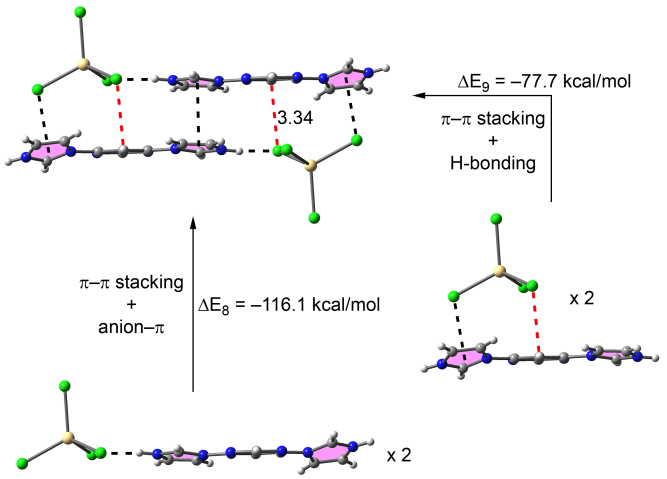

Fig. 17 Theoretical models and binding energies computed to evaluate the noncovalent interactions in compound **4**. Distance in Å.

We have also analyzed the interesting self-assembled dimer observed in the solid state of isomorphous compounds **4** and **5**. We have used the crystallographic coordinates of compound **4** as a model system. To evaluate the relative importance of the H-bonding and anion–π interactions involving the imidazole ring, we have computed the dimerization energies shown in Fig. 17. In both cases the π–π stacking interaction contributes to the interaction energy. That is, ΔE_8 accounts for the anion–π and π–π stacking interactions and ΔE_9 accounts for the H-bonding and π–π stacking interactions. As a result, by comparing both energies it can be concluded that each anion–π is 19.2 kcal/mol stronger [(ΔE_8-ΔE_9)/2)] than each H-bonding interaction likely due to the additional contacts of the chlorine atoms of the anion with the pyrimidinic ring (see red lines in Fig. 17) in the anion–π interaction.

Finally, we have used the Bader's theory of "atoms in molecules", which provides an unambiguous definition of chemical bonding, to further describe the noncovalent interactions presented above. The AIM theory has been successfully used to characterize and understand a great variety of interactions; therefore it is adequate to analyse the new interactions described above. In Fig. 18 we show the AIM analysis of the anion–π and lp–π assembly of compound **1** and the self-assembled dimer of compound **4**. As it can be observed for compound **1**, each anion–π interaction is characterized by the presence of one bond critical point (red spheres) that connects the chloride anion with one carbon atom of the imidazolium ring. The lp–π interaction is characterized by the presence of one bond critical point that connects the oxygen atoms of the water molecule with one nitrogen atom of the pyrimidinic ring. The whole assembly is further characterized by the presence of two ring critical points (yellow spheres) as a consequence of the concurrent anion–π/H-bonding/lp–π interactions that generate a macrocycle. In compound **4**, both anion–π interactions are characterized by the presence of three

CrystEngComm Accepted Manuscript

bond critical points that connect the chlorine atoms of the $ZnCl_4^{2-}$ anions with three carbon atoms of the diprotonated *bimipyr*H_2 cation (one from imidazole and two from pyrimidine ring). The π–π interaction is characterized by the presence of several bond and ring critical points that connect the antiparallel stacked imidazole rings and one nitrogen atom of the pyrimidine ring. The value of the Laplacian of the charge density computed at the bond critical points in both complexes is positive, as is common in closed-shell interactions.

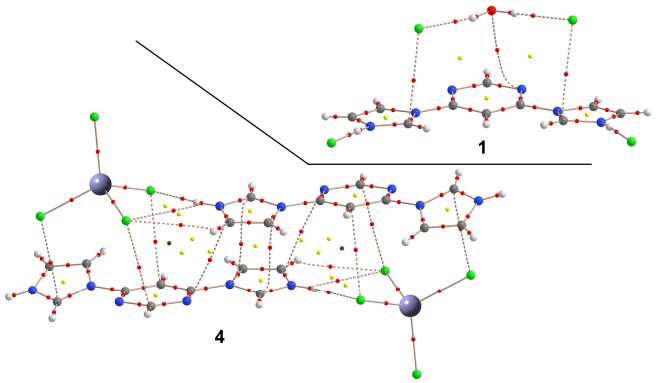

Fig. 18 AIM analysis of compounds **1** and **4**. Bond, ring and cage critical points are represented by red, yellow and green spheres, respectively. The bond paths connecting bond critical points are also represented by dashed lines.

Conclusions

We have synthesized and X-ray characterized five bis-N-imidazolylpyrimidine salts. The solid state structures show that the participation of the bis-N-imidazolylpyrimidine system in concurrent hydrogen bonding and anion–π interactions control the crystal packing. In all compounds, the anions are in close proximity to the electron deficient *bimipyr* core, forming distinctive anion–π interactions. Interestingly, the anions have the ability to link the cationic moieties together *via* anion–π interactions and provide useful supramolecular anion–π/π–π/π–anion type network for self-assembly progression. This experimental investigation gives support to the role of anion–π interactions in solid-state chemistry for building multi-dimentional structures. In addition, the computational study has been extended to the complexes, highlighting the impact of both the anion–π and trifurcated hydrogen bonding interaction on the final structure. Finally, the theoretical study of the energetic features of the noncovalent interactions is certainly important to gain knowledge in the intricate mechanism that governs the molecular recognition and crystal packing. To this respect, the assignment of discrete energy values to them can help to understand these mechanistic contributions to the crystal engineering community. In particular, the anion–π and hydrogen bonding interactions are especially relevant in the structures reported herein. Interestingly, in the complexes involving $[MCl_4]^{2-}$ anions, the ditopic anion–π interactions are energetically more favorable than the H-bonding interactions.

Acknowledgements

We thank the Ministerio de Economía y Competitividad (MINECO) of Spain (projects CTQ2011-27512/BQU, ENE2012-36368-C02-02 and CONSOLIDER INGENIO 2010 CSD2010-00065, FEDER funds) the Direcció General de Recerca i Innovació del Govern Balear (project 23/2011, FEDER funds) and Generalitat de Catalunya (grant 2014SGR-1643) for financial support. We thank the CTI (UIB) for computational facilities and allocation of computer time.

Notes and references

[a]Departament de Química, Universitat de les Illes Balears, Crta. de Valldemossa km 7.5, 07122 Palma de Mallorca (Baleares), Spain. E-mail: toni.frontera@uib.es; angel.garcia-raso@uib.es
[b]Institut de Ciència de Materials de Barcelona (CSIC), Campus UAB, 08193 Bellaterra, Spain.

† Electronic Supplementary Information (ESI) available: CCDC 1012937 – 1012941 contain the supplementary crystallographic data for this paper. See DOI: 10.1039/b000000x/

1 H. J. Schneider, *Angew. Chem., Int. Ed.* **2009**, *48*, 3924–3977; J.-M. Lehn, *Supramolecular Chemistry*; VCH: Weinheim, Germany, **1995**; J. W. Steed, J. L. Atwood, *Supramolecular Chemistry*; Wiley: Chichester, U.K., **2000**.

2 J. S. Murray, K. E. Riley, P. Politzer and T. Clark, *Aust. J. Chem*., 2010, **63**, 1598–1607; P. Politzer and J. S. Murray, *ChemPhysChem*, 2013, **14**, 278–294; P. Metrangolo and G. Resnati, *Cryst. Growth Des*., 2012, **12**, 5835–5838; P. Politzer, J. S. Murray and T. Clark, *Phys. Chem. Chem. Phys*., 2013, **15**, 11178; A Bauzá, T. J. Mooibroek and A. Frontera, *Angew. Chem. Int. Ed*. 2013, **52**, 12317; A. Bauza, T. J. Mooibroek and A. Frontera, *Chem. Eur. J*., 2014, **20**, DOI:10.1002/chem.201403680; A. Bauza, T. J. Mooibroek and A. Frontera, *Phys. Chem. Chem. Phys*. 2014, **16**, 10.1039/c4cp01983k.

3 G. R. Desiraju and T. Steiner, The Weak Hydrogen Bond in Structural Chemistry and Biology, Oxford Univ. Press, Oxford, 1999.

4 E. A. Meyer, R. K. Castellano and F. Diederich, *Angew. Chem. Int. Ed*. Engl., 2003, **42**, 1210; L. M. Salonen, M. Ellermann and F. Diederich, Ang*ew. Chem. Int. Ed*., 2011, **50**, 4808.

5 J. C. Ma and D. A. Dougherty, *Chem. Rev.,* 1997*,* **97**, 1303; N. Zacharias and D. A. Dougherty, *Trends Pharmacol. Sci.,* 2002*,* **23**, 281.

6 (a) A Frontera, P. Gamez, M. Mascal, T. J. Mooibroek and J. Reedijk*, Angew Chem. Int. Ed.,* 2011*,* **50**, 9564; (b) A. Bauzá, D. Quiñonero, P. M. Deyà and A. Frontera, *New J. Chem*., 2013, **37**, 2636–2641; (c) A. Bauzá, D. Quiñonero, P. M. Deyà and A. Frontera, *Chem. Phys. Lett*., 2013, **37**, 2636–2641.

7 D. Quiñonero, C. Garau, C. Rotger, A. Frontera, P. Ballester, A. Costa and P. M. Deyà, *Angew. Chem., Int. Ed*., 2002, **41**, 3389−3392.

8 (a) A. Frontera, F. Saczewski, M. Gdaniec, E. Dziemidowicz-Borys, A. Kurland, P. M. Deyà, D. Quiñonero and C. Garau, *Chem. Eur. J*. 2005, **11**, 6560−6567; (b) M. Mascal, Ang*ew. Chem., Int. Ed*., 2006, **45**, 2890−2893. (c) G. Gil-Ramirez, E. C. Escudero-Adan, J. Benet-Buchholz and P. Ballester, *Angew. Chem., Int. Ed*., 2008, **47**, 4114−4118. (d) B. L. Schottel, H. T. Chifotides and K. R. Dunbar, *Chem. Soc. Rev*., 2008, **37**, 68−83. (e) P. Gamez, T. J. Mooibroek, S. J. Teat and J. Reedijk, *Acc. Chem. Res*., 2007, **40**, 435−444. (f) A. Perez-Velasco, V. Gorteau and S. Matile, *Angew. Chem., Int. Ed*.,

CrystEngComm Accepted Manuscript

 This journal is © The Royal Society of Chemistry 2012

2008, **47**, 9603−9607. (g) R. E. Dawson, A. Hennig, D. P. Weimann, D. Emeryl, V. Ravikumar, J. Montenegro, T. Takeuchil, S. Gabutti, M. Mayor, J. Mareda, C. A. Schalley and S. Matile, *Nat. Chem*., 2010, **2**, 533−538.

9 (a) V. Gorteau, G. Bollot, J. Mareda, A. Perez-Velasco and S. Matile, *J. Am. Chem. Soc*., 2006, **128**, 14788–14789; (b) V. Gorteau, G. Bollot, J. Mareda and S. Matile, *Org. Biomol. Chem*., 2007, **5**, 3000–3012.

10 M. Mascal, A. Armstrong and M. D. Bartberger, *J. Am. Chem. Soc.* 2002, **124**, 6274−6276.

11 (a) A. Frontera, *Coord. Chem. Rev*. 2013, **257**, 1716–1727; (b) J. J. Fiol, M. Barceló-Oliver, A. Tasada, A. Frontera, A. Terrón and A. García-Raso, *Coord. Chem. Rev*., 2013, **257**, 2705–2715; (c) P. Gamez. *Inorg. Chem. Front*., 2014, **1**, 35–43.

12 (a) L. Adriaenssens, G. Gil-Ramírez, A. Frontera, D. Quiñonero, E. C. Escudero-Adán and P. Ballester, *J. Am. Chem. Soc*., 2014, **136**, 3208–3218; (b) O. B. Berryman, F. Hof, M. J. Hynes and D. W. Johnson, *Chem. Commun*., 2006, 506−508.

13 I. Alkorta, I. Rozas and J. Elguero, *J. Am. Chem. Soc*., 2002, **124**, 8593−8598.

14 (a) D. Kim, E. C. Lee, K. S. Kim and P. Tarakeshwar, *J. Phys. Chem. A*, 2007, **111**, 7980−7986. (b) B. Han, J. J. Lu and J. K. Kochi, *Cryst. Growth Des*., 2008, **8**, 1327−1334. (c) C. Estarellas, M. C. Rotger, M. Capo, D. Quinonero, A. Frontera, A. Costa and P. M. Deya, *Org. Lett*., 2009, **11**, 1987−1990.

15 (a) M. Mirzaei, H. Aghabozorg and H. Eshtiagh-Hosseini, *J. Iran. Chem. Soc*., 2011, **8**, 580; (b) M. Mirzaei, H. Eshtiagh-Hosseini, M. Chahkandi, N. Alfi, A. Shokrollahi, N. Shokrollahi and A. Janiak, *CrystEngComm*., 2012, **14**, 8468; (c) H. Eshtiagh-Hosseini and M. Mirzaei, *Mendeleev Commun*., 2012, **22**, 323; (d) P. Jaramillo, K. Coutinho and S. Canuto, *J. Phys. Chem. A*., 2009, **113**, 12485.

16 K. L. Han and G. Z. He, *J. Photochem. Photobiol. C Photochem. Rev*., 2007, **8**, 55.

17 (a) M. Pietrzak, M. F. Shibl, M. Broring, O. Kuhn and H. H. Limbach, *J. Am. Chem. Soc*., 2007, **129**, 296; (b) A. Dybala-Defratyka, P. Paneth, J. Z. Pu and D. G. Truhlar, *J. Phys. Chem. A*., 2004, **108**, 2475; (c) A. T. Colak, F. Colak, O. Z. Yesilel, D. Akduman, F. Yılmaz and M. Tumer, *Inorg. Chim. Acta*., 2010, **363**, 2149; (d) H. Eshtiagh-Hosseini, M. Mirzaei, N. Alfi, *Review on Proton Transfer Metal Complexes*, First Ed. (Lambert Academic Publishing GmbH & Co. KG., 2012).

18 (a) G. H. Cui, T. F. Liu and X. Peng, *J. Chem. Cryst*., 2011, **41**, 322; (b) X. Feng, J. Liu, T. F. Li and P. P. Lei, *Z. Kristallogr.-New Cryst. Struct*., 2011, 226, 80; (c) H. Aghabozorg, S. Omidvar, M. Mirzaei and B. Notash, *Z. Kristallogr.-New Cryst. Struct*., 2011, **226**, 123; (d) X. Feng, G. F. Li, T. F. Li and L. Y. Wang, *Synth. React. Inorg., Met.-Org., Nano-Met. Chem*., 2011, **41**, 250.

19 K. Harms and S. Wocadlo, XCAD4. University of Marburg, Marburg, Germany, 1995.

20 N. Walker and D. Stuart, *Acta Crystallogr., Sect. A: Found. Crystallogr.*, 1983, **39**, 158-166.

21 M. C. Burla, R. Caliandro, M. Camalli, B. Carrozzini, G. L. Cascarano, L. De Caro, C. Giacovazzo, G. Polidoria and R. Spagna, *J. Appl. Cryst*., 2004, **38**, 381-388.

22 G. M. Sheldrick, *Acta Crystallogr., Sect. A: Found. Crystallogr*., 2008, **64**, 112-122.

23 L. J. Farrugia, *J. Appl. Cryst*., 2012, **45**, 849-854

24 R. Ahlrichs, M. Bär, M. Häser, H. Horn and C. Kölmel, *Chem. Phys. Lett*., 1989, **162**, 165.

25 Spartan 10', v. 1.10, Wavefunction Inc, Irvin, CA, USA.

26 R. F. W. Bader, *Chem. Rev*., 1991, **91**, 893–928.

27 AIMAll (Version 13.05.06), Todd A. Keith, TK Gristmill Software, Overland Park KS, USA, **2013**.

28 (a) HypNMR 2008 program (Protonic Software; http://www.hyperquad.co.uk); (b) C. Frassineti, S. Ghelli, P. Gans, A. Sabatini, M. S. Moruzzi and A. Vacca, *Anal. Biochem.* **1995**, *231*, 374-382; (c) C. Frassineti, L. Alderighi, P. Gans, A. Sabatini, A. Vaccaand S. Ghelli, *Anal. Bioanal. Chem*. **2003**, *376*, 1041–1052.

29 B. Dong, T. Sakurai, Y. Bando, S. Seki, K. Takaishi, M. Uchiyama, A. Muranka and H. Maeda. *J. Am. Chem. Soc*., 2013, **135**, 14797–14805.

30 (a) P. C. Junk, C. J. Kepert, L. I. Semenova, B. W. Skelton and A. H. White, *Z. Anorg. Allg. Chem*., 2006, **632**, 1293; (b) F. C. Krebs, B. W. Laursen, I. Johanssen, A. Faldt, K. Bechgaard, C. S. Jacobsen, N. Thorup and K. Boubekur, *Acta Crystallogr*., 1999, **B55**, 410; (c) N. S. al-Zamil, E. H. M. Evans, R. D. Gillard, D. W. James, T. E. Jenkins, R. J. Lancashire and P. A. Williams, *Polyhedron*, 1982, **1**, 525; (d) J. Rozière, M. S. Lehmann, J. Potier, Acta Crystallogr. 1979, B35, 1099; (e) J. Rozière, M.T. Rozierè-Boriès, J. M. Williams, *Inorg. Chem*., 1976, **15**, 2490; (f) J. M. Williams, N. Dowling, R. Gunde, D. Hadzi, B. Orel, *J. Am. Chem. Soc*., 1976, **98**, 1581; (g) B. D. Faithful and S. C. Wallwork, *Chem. Comm*., 1967, 1211; (h) G. C. Dobinson, R. Mason, D. R. Russell, *Chem. Comm*., 1967, 62; (i) G. Thevenet and N. Rodier, *Acta Crystallogr*., 1978, **B34**, 880.

31 M. Torres, P. Cañellas, C. Estarellas, A. García-Raso, J. J. Fiol, F. M. Albertí, A. Frontera, E. Molins, I. Mata and P. M. Deyà, *Tetrahedron*, 2012, **68**, 2374–2382

32 P. Manna, S. K. Seth, A. Bauzá, M. Mitra, S. R. Choudhury, A. Frontera and S. Mukhopadhyay, *Cryst. Growth Des.*, 2014, **14**, 747–755

33 P. Manna, S. K. Seth, A. Das, J. Hemming, R. Prendergast, M. Helliwell, S. R. Choudhury, A. Frontera and S. Mukhopadhyay, *Inorg. Chem.*, 2012, **51**, 3557–3571.

CrystEngComm Accepted Manuscript